Saudi Journal of Biological Sciences 27 (2020) 556–560

Contents lists available at ScienceDirect

Saudi Journal of Biological Sciences

journal homepage: www.sciencedirect.com

Original article

Construction and analysis of finite element model of defected articular cartilage

Yuan Lin, Jizheng Qin, Honghai Zhao, Chun Xia *

Department of Joint Surgery & Sports Medicine, Zhongshan Hospital Xiamen University, Xiamen 361004, China

ARTICLE INFO

Article history:
Received 24 September 2019
Revised 13 November 2019
Accepted 18 November 2019
Available online 25 November 2019

Keywords:
Articular cartilage
Finite element simulation
Fluid flow
MRI
Permeability

ABSTRACT

In order to construct a finite element model of defected articular cartilage, the mechanical behavior and degeneration of articular cartilage after injury were studied. The simplified analytical models of normal and defected articular cartilage and finite element models were established, respectively. Firstly, the analytical solution model and finite element model of hollow defect were constructed by using the elasticity theory of multi-hollow medium. Then, the analytical results of each model were calculated and programmed. The software MATLAB was used for programming calculation. Finally, a finite element solid model of defected articular cartilage was established by using human femoral joint. The solid model was analyzed and calculated by magnetic resonance imaging (MRI). The results showed that when the radius of articular cartilage defect r = 0, i.e. there was no defect in articular cartilage, the internal pore pressure of the defect cartilage was the largest, and its pore pressure value was 27×10^3pa. When the depth of articular cartilage defect r = 0, i.e. there was no defect in articular cartilage, the internal pore pressure of the defect cartilage was the largest, and its pore pressure value was 27.5×10^3pa, and it gradually decreased towards the outer boundary of cartilage. When the surface of femoral cartilage began to defect, with the increase of the depth of the defect (from shallow to deep), the maximum pore pressure in the defect cartilage gradually decreased, but the speed is slowly. With the increase of the defect radius, that is, the area of the defect, the maximum pore pressure in the defect cartilage gradually decreased. When there was no defect of articular cartilage, the internal pore pressure of the defect cartilage was the maximum, the value of pore pressure was 8.7×10^3pa, the value of pore pressure at the contact position of femoral cartilage was the largest, and it gradually decreased towards the outer boundary of cartilage. At the same location, the pore pressure of normal cartilage was significantly higher than that of defected cartilage. With the change of defect location, the pore pressure was reduced accordingly. Moreover, when the defect position moved from the outside to the inside, the corresponding pore pressure value was decreased gradually. To sum up, the finite element model of defected articular cartilage based on porous elasticity theory has better calculation ability, which proves the validity of the finite element software, and provides a strong basis for future model establishment and clinical treatment of articular cartilage.

1. Introduction

Articular cartilage covers the surface of the bone in the joint. Some are hyaline cartilage and some are fibrocartilage (Liu et al., 2018). It belongs to a special kind of solid connective tissue and the cartilage itself has elasticity. The articular cartilage faces the articular cavity very smoothly, avoiding the wear and tear of the bone during exercise (Liu et al., 2017). Higher deformation characteristics can also provide as much bone contact area as possible, buffer the stress between bones in the process of stress, and avoid the damage to joint bone and the damage of bone caused by stress concentration during stress process (Manda and Eriksson, 2014). The basic cause of cartilage injury is that the biomechanical properties of some parts of the joint cannot adapt to the stress field caused by abnormal loads. Therefore, the study of cartilage flow behavior and the analysis of cartilage stress by biomechanics are

* Corresponding author.
E-mail address: huixia186897@126.com (C. Xia).

Peer review under responsibility of King Saud University.

Production and hosting by Elsevier

https://doi.org/10.1016/j.sjbs.2019.11.020

of great significance to understand the nature of cartilage and the mechanism of cartilage degradation (Zha et al., 2017; Halonen et al., 2014). This will further promote the study of bionic cartilage substitutes and provide theoretical analysis and relevant important reference basis for experimental or finite element simulation methods for the clinical treatment of various knee cartilage injuries (Frisbie et al., 2015; Zhao et al., 2015; Mumme et al., 2016). Therefore, the biomechanical study of articular cartilage is of great significance (Tomic et al., 2018) (see Fig. 1).

The degeneration of articular cartilage can lead to arthritis. The cartilage itself has some shortcomings, such as less blood vessels, fewer cells, dispersed cell distribution and low repair ability. However, in cartilage defect repair, whether perichondrium tissue engineering or cartilage transplantation, the mechanical environment of cartilage itself will affect the effect of cartilage repair (Behrou et al., 2017). In animal experiments, only the effect of the form of cartilage defect on the stress distribution of cartilage around cartilage defect was studied (Matsuoka et al., 2017; Bosch et al., 2017). Klets et al. used magnetic resonance imaging (MRI) and finite element software to establish isoelastic, isoporous and elastic cartilage. The simulation of linear elastic model deviates most from the actual situation. Therefore, the study of cartilage as a porous two-phase elastic material and the establishment of a real human cartilage simulation model are another focus of this research (Singh et al., 2017).

Based on the above research background, the simplified analytical models of normal and defected articular cartilage and finite element model were established, the mechanism of articular cartilage degeneration was explored by setting up the defect degeneration, respectively. The changes of mechanical behavior and the degeneration law of articular cartilage defects after articular cartilage injury were discussed. It was found that the pore pressure and velocity around the defect decreased with the increase of the defect depth and radius. The change of pore pressure and flow velocity around the defect would decrease gradually as the defect moved from the outside to the inside, so as to provide a strong basis for the establishment of future models and clinical treatment of articular cartilage. Through the application of this model, the computer mathematical model of muscle soft tissue joint will be added in the future research, so as to carry out more accurate mechanical research.

2. Methods

2.1. Establishment and solution of mathematical model

Based on Biot's theory, elasticity of porous media has been developed. The following formulas can be used to describe the elastic behavior of cartilage in porous media. According to previous research and experiments, in general, the flat cylinder model of articular cartilage is set up to establish a porous elastic model of articular cartilage based on cylindrical coordinates.

Constitutive relationship:

$$\sigma_{ij} = C_{ijkl}\varepsilon_{kl} - \alpha_{ij}p \tag{1}$$

$$p = M(\xi - \alpha_{ij}\varepsilon_{ij}) \tag{2}$$

Darcy's law:

$$q_i = -\frac{k_{ij}}{\mu}\left(p_{,i} + \rho_f \ddot{u}_i^s\right) \tag{3}$$

In the above formula, σ_{ij} indicates the total stress, ε_{kl} refers to the total strain tension, and p is the pressure of the bone unit. α_{ij} is the coefficient tensor of Biot, and M is the modulus of Biot. C_{ijkl} is the elastic coefficient tensor, ξ is a variable of the liquid, $\ddot{u}_i^s$ is a second derivative, ρ suggests the density, k_{ij} denotes the tensor of permeability coefficient, and μ is the coefficient of liquid viscosity.

The velocity of liquid can be determined by Darcy's law. To sum up, the analytical solution of pressure and velocity under case II is as follows:

$$P^{II}(z,t) = \varepsilon_z 0\left[\left(\frac{C_{11}}{1+\alpha} + \alpha M\right)\frac{\cosh(\alpha z)}{\cosh(\alpha h)} - \alpha M\right]e^{i\omega t} \tag{4}$$

$$q^{II}(z,t) = \frac{k}{\mu}\varepsilon_z 0\left[\left(\frac{C_{11}}{1+\alpha} + \alpha M\right)\frac{a\sinh(\alpha z)}{\cosh(\alpha h)}\right]e^{i\omega t} \tag{5}$$

Combined with Darcy's law, the analytical solutions of pressure and velocity are as follows:

$$P^{II}(r,t) = \left[-\frac{MC_{11}\alpha(C_3+\varepsilon_{z0})}{C_{11}+M\alpha^2} + A_3I_0(Cr) + B_3K_0(Cr)\right]e^{i\omega t} \tag{6}$$

$$q^{III}(r,t) = -\frac{kC}{\mu}[A_3I_1(Cr) - B_3K_1(Cr)]e^{i\omega t} \tag{7}$$

The analytical solutions of pressure and velocity of hollow damaged/defective articular cartilage under the second boundary condition are as follows.

$$P^{IV}(r,t) = \left[-\frac{MC_{11}\alpha(C_4+\varepsilon_{z0})}{C_{11}+M\alpha^2} + A_4I_0(Cr) + B_4K_0(Cr)\right]e^{i\omega t} \tag{8}$$

$$q^{IV}(r,t) = -\frac{kC}{\mu}[A_4I_1(Cr) - B_4K_1(Cr)]e^{i\omega t} \tag{9}$$

2.2. Establishment of finite element model

The finite element cartilage model was established by using Comsol Multiphysics finite element software. Firstly, the normal

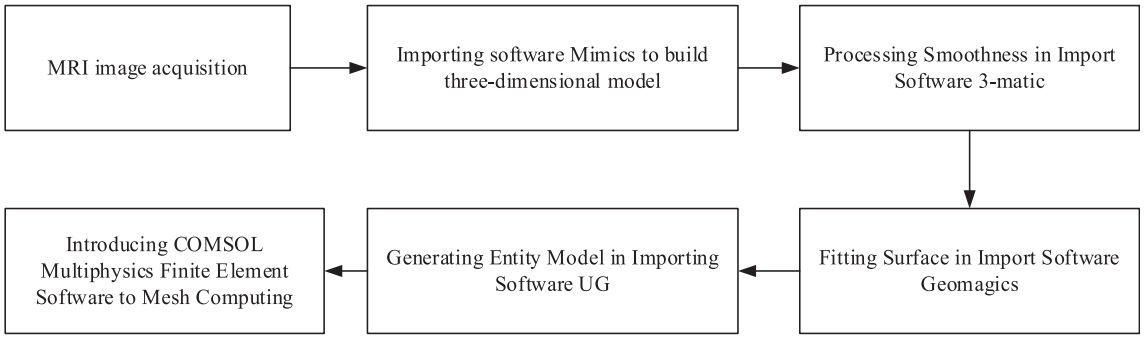

Fig. 1. Schematic diagram of modeling steps.

cartilage cylinder model was established, and then the defected cartilage cylinder model was established. According to the theoretical deduction hypothesis, the boundary conditions, external loads and geometric settings of the finite element model are also two-dimensional axisymmetric settings. For normal cartilage model and defected cartilage model, two kinds of boundary conditions, i.e. confined conditions and non-confined conitions, are set simultaneously, and then the pore pressure of cartilage model is calculated. Table 1 shows the physical parameters of normal cartilage model and defected cartilage model.

According to the theoretical deduction, the assumed boundary conditions are consistent with those of the finite element model. The normal cartilage model cannot penetrate the subchondral surface because of its fixed axial displacement under non-confined boundary conditions. The surrounding can be permeated and moved freely, and the upper surface cannot be permeated by applying axial displacement constraints. The defected cartilage model is similar to the normal cartilage model in that the axial displacement of the subchondral surface is fixed and cannot penetrate, and the surrounding cartilage can penetrate and move freely. Under the boundary condition of the defect cartilage model, the lower surface of the defect cannot penetrate and rigid constraints are impossible, and the surrounding boundary cannot penetrate with rigid constraints. The inner surface of the defect can move freely and permeate freely.

2.3. Establishment of ideal cartilage model

According to the experimental requirements, the cartilage models of femoral cartilage, tibial plateau cartilage and meniscus were constructed. Because the material, shape, boundary conditions and force acting on cartilage of the normal cartilage model established in this paper belonged to the form of axial symmetry, COMSOL Multiphysics finite element software was used to analyze and construct the data, to study the porous elasticity of cartilage defect and degeneration. Only when the influence of defect location on cartilage defect is studied can the three-dimensional idealized model be used to study it.

The following table is the relevant parameters of cartilage defect of ideal model. The outer radius of femoral cartilage model is set at 17.0 mm, the thickness of cartilage is set at 2.5 mm, and the thickness of cartilage layer is set at about 5% of cartilage. Draw the sketch of two-dimensional axisymmetric model directly in UG modelling environment, then export the DXF file, and then use COMSOL Multiphysics software to analyze and calculate the vector data in the derived DXF file. In UG environment, the two-dimensional section of each part is rotated and then the entity is constructed, and this model is a three-dimensional model. The STP format file is imported from UG environment, and then the data of the three-dimensional object is analyzed and calculated by COMSOL Multiphysics software (see Table 2).

2.4. The establishment of defect degenerated cartilage model

The cartilage model was influenced by geometric factors such as femoral defect and the cartilage model was also studied. As shown in the table below, the radius, depth and location of the defect cartilage were numbered, set and calculated. In the process of cartilage degradation, the elastic modulus of cartilage begins to decrease and the permeability increases. According to the related research, the physical parameters of femoral degeneration were studied, and the influence of the parameters of cartilage model on pore pressure was studied (see Table 3).

2.5. Construction of finite element model of articular cartilage

MRI was performed on the knee joint of healthy adult males. Medical image atlas of coronal and sagittal knee joints was collected. Then, the articular cartilage of knee joints was modeled by Mimics 19.0 modeling software. After the model was established, it was imported into 3-matic software for processing. In order to make the model smoother and easier to analyze and calculate, the model can be imported into the CAD module of Geomagic studio 12.0 for comprehensive optimization. To transform the three-dimensional model into a solid surface, the three-dimensional model was divided into surface patches, grids were constructed, and finally the surface was fitted and stitched. The modeling steps are as follows:

In modeling, it mainly includes image acquisition, two-dimensional image import, threshold segmentation, intelligent expansion and calculation of contour line, calculation of 3D model, derivation of three-dimensional model, 3-matic software modification model, Geomagic Studio software fitting surface, UG software generating entity model and COMSOL Multiphysics software finite element calculation, etc.

3. Results

3.1. Change of defect area

As can be seen from the following figure, when the radius of articular cartilage defect was r = 0, i.e. the articular cartilage did not produce defects, the pore pressure inside the defect cartilage was the largest, and its pore pressure value was 27×10^3pa, and gradually decreased to the outer boundary of the cartilage; when r = 1.5 mm, the pore pressure inside the defect cartilage was 23×10^3pa; when r = 2.5 mm, the pore pressure inside the defect cartilage was 20×10^3pa; when r = 3.5 mm, the pore pressure inside defected cartilage was 17×10^3pa; when r = 4.5 mm, the pore pressure inside defected cartilage was 13×10^3pa. It can be seen that the maximum pore pressure in the defect cartilage decreases with the increase of the radius of the defect, that is, the area of the defect (see Fig. 2).

3.2. Change of defect depth

As can be seen from the following figure, when the depth of articular cartilage defect was r = 0, i.e. no articular cartilage defect occurred, the pore pressure inside the defected cartilage was the largest, and its value was27.5×10^3pa. The pore pressure in the contact part between meniscus and femoral cartilage began to decrease gradually towards the cartilage boundary, while the pore pressure outside the cartilage boundary was the smallest, and its value was zero. With the increase of defect depth, when d = 0.5 mm, the pore pressure inside defected cartilage was 24×10^3pa; when d = 1 mm, the pore pressure inside defected

Table 1
Geometry parameters of the models (mm).

Category	Radius R	Internal diameter a	External diameter b	Height h
Normal cartilage model	6	/	/	2.5
Defected cartilage model	/	2.5	6	2.5

Table 2
Relevant parameters of cartilage defect.

Parameters	Porosity	Biot coefficient α	Compressibility $\chi_f(1/Pa)$	Dynamic viscosity μ	Liquid density $\rho_s(kg/m^3)$
Femoral cartilage Tibial plateau cartilage Meniscus	0.27	1	4.4526	0.00152	1000

Table 3
Degree of freedom of defect radius, defect depth and defect location.

No.	Defect radius (mm)	Freedom	Defect depth	Freedom	Defect location	Freedom
1	1.5	102,451	Shallow	102,584	Outside	604,798
2	2.5	100,852	Medium	102,562	Near the outside	652,795
3	3.5	99,659	Deep	102,041	Near the inside	654,357
4	4.5	99,103	Whole layer	102,636	Inside	652,484

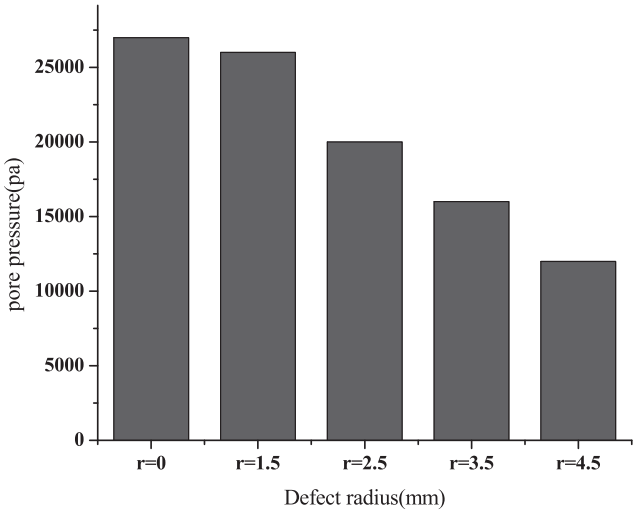

Fig. 2. Maximum pressure histogram of cartilage with different radius of defect.

cartilage was 23×10^3pa; when d = 1.5 mm, the pore pressure inside defected cartilage was 22.5×10^3pa; when d = 2 mm, the pore pressure inside defected cartilage was 22×10^3pa. It can be seen from this that when the surface of femoral cartilage began to have defect, and with the increase of defect depth (from shallow to deep), the maximum pore pressure inside the defect cartilage gradually decreases, but slowly (see Fig. 3).

3.3. Change of defect location

As can be seen from the figure below, when the articular cartilage was not defected, the pore pressure inside the defected cartilage was the largest, its pore pressure value was 8.7×10^3pa, and the pore pressure at the contact position of femoral cartilage was the largest, and gradually decreased to the outer boundary of the cartilage; when the deviated 0.5 mm to the center, the pore pressure in the defect cartilage was 7.8×10^3pa; when the defect deviated 1 mm to the center, the pore pressure in the defect cartilage was 7.6×10^3pa; when the defect deviated 1.5 mm to the center, the pore pressure in the defect cartilage was 7.3×10^3pa. It can be seen that when the location of cartilage defect moves gradually from medial to lateral, the pore pressure also decreases gradually (see Fig. 4).

3.4. Changes of pore pressure in normal cartilage and defected cartilage

Because of various reasons, different groups of people have different parts of articular cartilage, different people have different

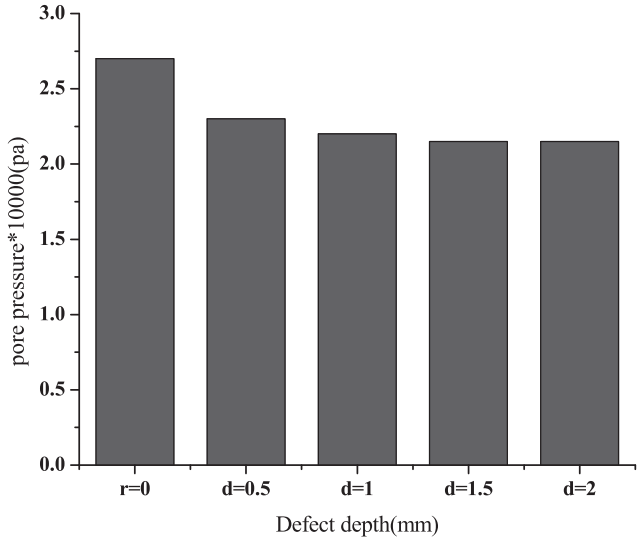

Fig. 3. Maximum cartilage pressure histogram with different depth of defect.

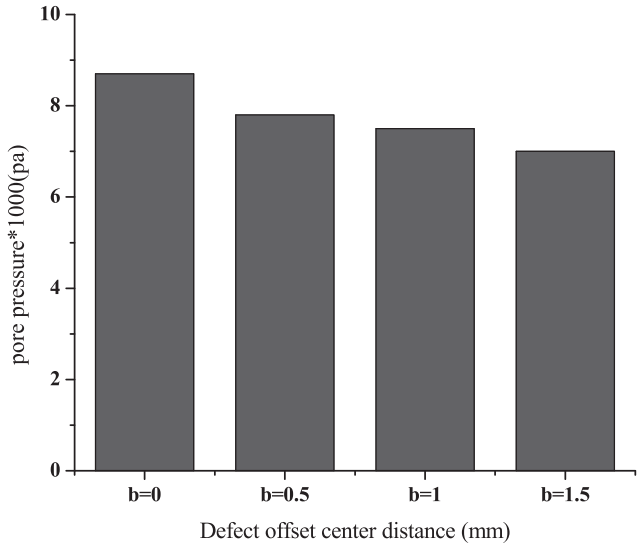

Fig. 4. Maximum pressure histogram of cartilage at different defect locations.

parts of articular cartilage defects. When the location of cartilage defect moved gradually from lateral to medial, the location of cartilage defect was recorded as 1, 2, 3 and 4 at equal intervals. As can be seen from the figure below, at the same location, the pore

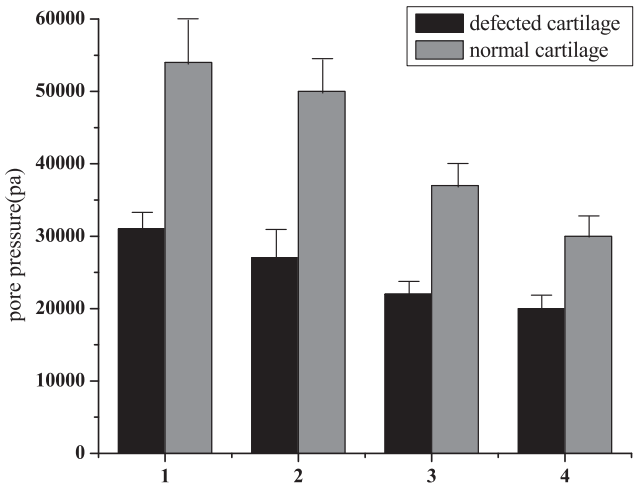

Fig. 5. Pressure histogram of normal cartilage and defected cartilage with different defect locations under pulsating displacement load.

pressure of normal cartilage was significantly greater than that of defected cartilage. With the change of defect location, the pore pressure should be reduced accordingly. Moreover, when the defect position moved from the outside to the inside, the corresponding pore pressure value was decreased gradually (see Fig. 5).

4. Discussion

The simplified analytical models of normal and defected articular cartilage and finite element model were established, respectively. Firstly, the analytical solution model and finite element model of hollow defect were constructed by using the elasticity theory of multi-hollow medium. Then, the analytical results of each model were calculated and programmed. An ideal cartilage model was established. On the basis of the research on the defect and degeneration of femoral cartilage, the finite element model of human femoral articular cartilage was established by using MRI image for calculation and analysis. The control variable method was used to establish different geometric defect and physical degradation models for the finite element model. The changes of pore pressure and flow velocity between normal cartilage and defect cartilage under pulsating load were compared.

The experimental results showed that the pore pressure and flow velocity around the defect decreased with the increase of defect radius. The articular cartilage model with the physical parameters of cartilage degeneration changed was set up. With the decrease of the elastic modulus of articular cartilage, the pressure and flow velocity in the pore pressure concentration area of cartilage gradually decreased. The change of pore pressure and flow velocity around the defect decreased gradually as the defect moved from the outside to the inside. With the formation and increase of defects, the decrease of pore pressure and flow velocity in cartilage would lead to the decrease of chondrocyte metabolism, and the corresponding metabolism of biochemical factors would be affected. Because there were almost no blood vessels in cartilage, only exchange with the fluid outside the matrix to metabolize, the degradation of cartilage defects would further accelerate the apoptosis of chondrocytes, which would lead to the decrease of collagen fiber and proteoglycan content of cartilage, and further damage of cartilage. This study proved the validity of the finite element software. The application of the model software could further realize the biological mechanism of articular cartilage and provide reliable basis and guidance for the treatment of clinical joint diseases. The results of the two methods were basically consistent, which proved the validity of the finite element software.

However, there are still some limitations and shortcomings in this study. Firstly, articular cartilage is actually an anisotropic heterogeneous biomaterial whose physical properties change with the change of deformation. In this experiment, the effect of collagen fibers is not considered separately in the model. Actual cartilage can exhibit porous viscoelastic properties at the same time. Then, the actual force of human body in walking and running is more complex, not only with axial load, but also with sliding and rolling. Therefore, the theoretical and experimental research on the degradation mechanism of articular cartilage injury needs to be further deepened. In the future research, based on the real cartilage finite element model, the viscoelastic properties of porous cartilage can be calculated and set up.

References

Liu, H., Zhao, Y., Zhao, S., et al., 2018. Analysis of the stress state in articular cartilage defect repairing area. J. Biomed. Eng. 35 (5), 705.
Liu, H.Y., Duan, H.T., Zhang, C.Q., et al., 2017. Study of the mechanical environment of chondrocytes in articular cartilage defects repaired area under cyclic compressive loading. J. Healthcare Eng. 2017 (1), 1–10.
Manda, K., Eriksson, A., 2014. Modeling of constrained articular cartilage growth in an intact knee with focal knee resurfacing metal implant. Biomech. Model. Mechanobiol. 13 (3), 599–613.
Zha, G., Li, X., Niu, X., et al., 2017. Application of Collagen-β-tricalcium phosphate complex for repairing articular cartilage defects. J. Biomater. Tissue Eng. 7 (3), 241–247.
Halonen, K.S., Mononen, M.E., Jurvelin, J.S., et al., 2014. Deformation of articular cartilage during static loading of a knee joint – Experimental and finite element analysis. J. Biomech. 47 (10), 2467–2474.
Frisbie, D.D., Mccarthy, H.E., Archer, C.W., et al., 2015. Evaluation of articular cartilage progenitor cells for the repair of articular defects in an equine model. J. Bone Joint Surgery American 97 (6), 484–493.
Zhao, M., Chen, Z., Liu, K., et al., 2015. Repair of articular cartilage defects in rabbits through tissue-engineered cartilage constructed with chitosan hydrogel and chondrocytes. J. Zhejiang Universityence B 16 (11), 914–923.
Mumme, M., Barbero, A., Miot, S., et al., 2016. Nasal chondrocyte-based engineered autologous cartilage tissue for repair of articular cartilage defects: an observational first-in-human trial. Lancet 388 (10055), 1985–1994.
Tomic, A., Grillo, A., Federico, S., 2018. Poroelastic materials reinforced by statistically oriented fibres—numerical implementation and application to articular cartilage. IMA J. Appl. Math. 79 (5), 1027–1059.
Behrou, R., Foroughi, H., Haghpanah, F., 2017. A novel study of temperature effects on the viscoelastic behavior of articular cartilage. J. Mech. Behav. Biomed. Mater. 78, 214–223.
Matsuoka, M., Onodera, Tomohiro, Homan, Kentaro, et al., 2017. Depletion of gangliosides enhances articular cartilage repair in mice. Sci. Rep. 7, 43729.
Bosch, M.H.V.D., Ramos, Y.F., Hollander, W.D., et al., 2017. Increased expression of CCN4/WISP1 in osteoarthritic articular cartilage is epigenetically regulated and disrupts cartilage homeostasis. Osteoarthritis Cartilage 25 (1), S38.
Singh, P.N., Yadav, U.S., Azad, K., et al., 2017. Regulatory roles of NFIA and GATA3 in embryonic articular and transient cartilage differentiation. Mech. Dev. 145, S97.